# Fermi surface formed by zone folding in the stage-2 InCl₃ graphite intercalation compound

W. R. Datars, J. D. Palidwar, T. R. Chien, and P. K. Ummat

*Department of Physics and Astronomy, McMaster University, Hamilton, Ontario, Canada L8S 4M1*

H. Aoki and S. Uji

*National Research Institute for Metals, 1-2-1 Sengen, Tsukuba, Ibaraki 305, Japan*
(Received 25 April 1995; revised manuscript received 10 July 1995)

The de Haas–van Alphen (dHvA) effect of the stage-2 InCl₃ graphite intercalation compound was studied with two dHvA spectrometers, one providing fields up to 14 T and temperatures between 50 and 800 mK and the other up to 5.5 T in the temperature range 1.5–4.2 K. Fifteen dHvA frequencies were measured along with the cyclotron masses of many of them. The frequencies were explained by the zone folding of the two Fermi-surface cylinders of the stage-2 compound. The orbits were formed by translation of the $8\sqrt{3} \times 8\sqrt{3}R30°$ lattice of the intercalant molecules.

## I. INTRODUCTION

The hole carriers in a stage-2 graphite intercalation compound (GIC) are expected to occupy two energy bands.[1] They are located at the corners of the hexagonal Brillouin zone of the graphite lattice and are in Fermi-surface cylinders directed along the $c$ axis. The cross-sectional area of the cylinders is small relative to the area of the hexagonal surface of the graphite Brillouin zone.

If the intercalant molecules have an ordered arrangement they form a superlattice on the hexagonal carbon arrangement. The Brillouin zone of the superlattice is much smaller than the graphite Brillouin zone when the lattice vectors of the superlattice are a multiple of the graphite lattice vectors. The Fermi surface can be translated by the reciprocal lattice vectors of either periodicity. Thus the Fermi surface can be translated by the reciprocal lattice vectors of the superlattice. This results in the overlap of the Fermi surface from neighboring translations, which permits the coupling of the carrier orbits. This process is called zone folding.

Recently it has been shown that a superlattice formed in the stage-2 InCl₃ GIC.[2] The ordering transition detected by the resistivity occurred at 155 K during the first time a sample was cooled from room temperature. This long-range order existed at room temperature after the sample had been cooled. The unit cell determined by x-ray diffraction of intercalated single crystals was $(4\sqrt{3} \times 4\sqrt{3})R30°$ with respect to the hexagonal carbon lattice.

The purpose of this paper is to show how zone folding in the stage-2 InCl₃ GIC affects the Fermi surface. It causes a multitude of orbits that were detected by the de Haas–van Alphen (dHvA) effect in magnetic fields up to 13.8 T. There is excellent agreement between the predicted and measured cross-sectional areas of the Fermi-surface pieces.

In Sec. II the synthesis of the intercalated graphite compound and the experimental methods are discussed. In Sec. III the experimental results of the de Haas–van Alphen experiments conducted over field ranges of 7.7–13.8 T and 2–5 T are given. In Sec. IV the techniques used to calculate the dHvA frequencies from zone folding are described in detail

and a comparison between these calculated values and those determined experimentally is discussed.

## II. EXPERIMENTAL METHOD

The stage-2 InCl₃ GIC samples were prepared by reacting InCl₃ with highly oriented pyrolytic graphite in a Cl₂ atmosphere at a pressure of 2 atm for 18 days.[3] They were determined to be in a stage 2 with the $c$ axis repeat distance $I_c = 12.8$ Å from (001) x-ray diffraction showing that there were no traces of other stages and that the $c$-axis ordering was excellent by the narrow sharp diffraction lines.[2]

The dHvA experiments with sample 1 were done with the sample in a 14-T superconducting magnet and cooled by a top-loading dilution refrigerator with a base temperature of 25 mK.[4] The measurements were performed with a sample temperature of between 50 to 800 mK. Such low temperatures were part of the operating system but were not necessary because the cyclotron masses of the carriers are low. It was difficult to determine the cyclotron masses accurately because the change of the dHvA amplitude was small at the temperatures of less than 0.8 K, which were easily accessible. However, the use of magnetic fields up to 14 T permitted the determination of low and high dHvA frequencies. The dHva oscillations with the smaller frequencies were detectable down to 2 T.

The results for sample 1 exhibited many dHvA frequencies that had to be confirmed with more samples. Since the measurements could be done at low fields and at temperatures up to 4.2 K, measurements with samples 2 and 3 were carried out with a 5.5-T superconducting solenoid and temperatures 1.5–4.2 K.[4] This temperature range was useful for the measurements of the cyclotron masses. The sensitivities of the two dHvA systems were similar. In both systems the sample was placed in a detection coil that could be rotated to set the angular position of the sample.

## III. EXPERIMENTAL RESULTS

The dHvA spectrum of sample 1 from data taken in the magnetic-field range 7.7–13.8 T is shown in Fig. 1. There are at least 15 dHvA frequencies between 127 and 1424 T.
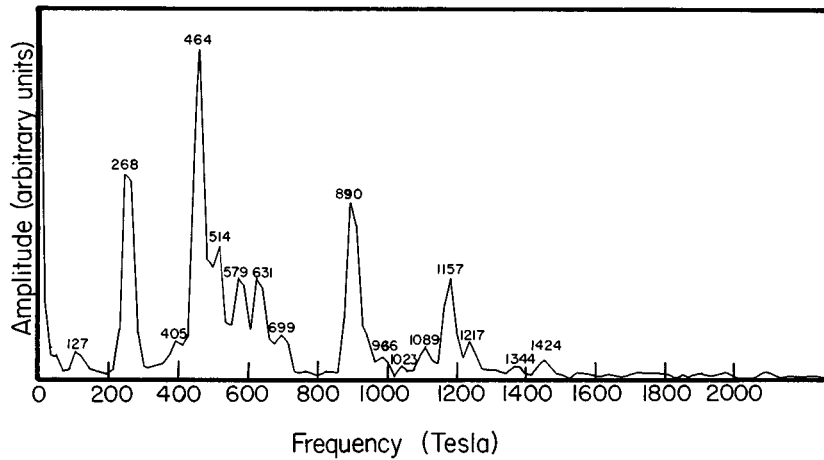
FIG. 1. dHvA of sample 1 over magnetic-field range 7.7–13.8 T.

The peak at 405 T is omitted from Table I because it was not reproducible in the other dHvA spectra. The dHvA spectrum of sample 2 from data taken in the field range 2–5 T is shown in Fig. 2. The resolution is better in Fig. 2 and peaks at 127, 268, 464, and 840 T in Fig. 1 are confirmed in Fig. 2 to within 2 T. The spectrum for sample 3 was very similar to that of sample 2 shown in Fig. 2 and confirmed the frequencies that are reported.

The cyclotron masses were determined from the temperature dependence of the Fourier amplitude of the dHvA frequencies. The measured dHvA frequencies and cyclotron masses are given in Table I.

The angular dependence of the dHvA frequencies on the angle $\theta$ between the magnetic-field direction and the $c$ axis was measured for the range $\theta < 20°$ in which the dHvA effect was observable. The frequencies followed the relation $f = f_0 \sec\theta$, showing that all the orbits are on cylindrical Fermi-surface pieces.

TABLE I. de Haas–van Alphen frequencies in units of Tesla for three samples of the stage-2 InCl$_3$ GIC and cyclotron masses in units of the free-electron mass.

| Field range ($T$) Temperature (K) | dHvA Frequency (T) | | | |
| | Sample 1 7.7–13.8 0.050 | Sample 2 2.5–4.5 4.2 | Sample 3 2–5 1.5 | Cyclotron mass ($m^*/m$) |
| --- | --- | --- | --- | --- |
| | 127 | 127 | 126 | 0.095 |
| | 268 | 271 | 268 | 0.096 |
| | 464 | 468 | 465 | 0.138 |
| | 514 | 518 | 514 | 0.120 |
| | 579 | 581 | 578 | 0.158 |
| | 631 | | | |
| | 699 | 710 | 708 | 0.192 |
| | 890 | 893 | 890 | 0.22 |
| | 966 | | | |
| | 1023 | | | |
| | 1089 | | | |
| | 1157 | | | 0.27 |
| | 1217 | | | |
| | 1344 | | | |
| | 1424 | | | 0.27 |

## IV. ANALYSIS AND DISCUSSION

The ($hk0$) x-ray diffraction study determined that the InCl$_3$ molecules form a superlattice with lattice parameters of $(4\sqrt{3} \times 4\sqrt{3})R30°$ with respect to the graphite lattice vectors after a sample has been cooled to 4 K. This superlattice allows for the reciprocal space translation of the cylindrical graphite Fermi surfaces located at the $U$ and $U'$ points of the graphite Brillouin zone to the $O$ point of the intercalant Brillouin zone. It is the overlap of these cylinders from different translations that enables the determination of the zone folding of the fundamental de Haas–van Alphen frequencies into many frequencies as a result of Bragg reflections. The determination of these orbits is done by drawing the fundamental orbits (circles in two dimensions) at the $O$ points of the first, second, and third Brillouin zones of the intercalant superlattice. The orbits created by the overlap of these circles are then considered as possible carrier orbits and their calculated areas are compared to those observed through dHvA. The radius of the circles is adjusted to provide the most suitable orbital overlaps as long as the frequency represented by this radius remains reasonable. If a piece with mixed curvature of the sides was considered to be
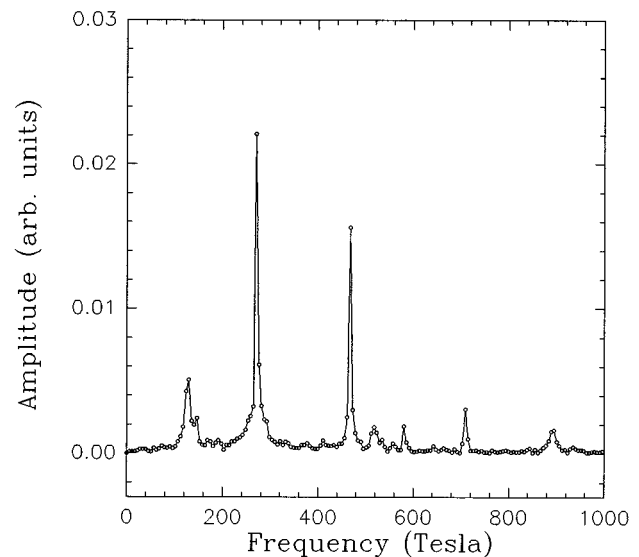


FIG. 2. dHvA of sample 2 over magnetic-field range 2–5 T.

an orbit, the carriers responsible for this piece would have to switch between electrons and holes and this is not allowable. Thus the rule in determining that a given path is allowable is that the curvature of all sides that contribute to the piece must be the same. Since we are dealing with an acceptor compound, the pieces that have sides with positive curvature are attributed to hole orbits and those with negative curvature are attributed to electron orbits. In addition to the pieces directly resulting from the overlap of circles, these pieces can be coupled together to allow for extended orbits through reciprocal space. The same rule applies to these extended pieces as for the uncoupled pieces in that only pieces consisting of one type of curvature can be considered to be possible carrier orbits.

Our zone-folding model does not include any interaction between the orbits. Interaction results in energy gaps at the intersections of orbits where there is degeneracy. These gaps would have to be crossed with the assistance of magnetic breakdown.[5] However, there is no direct evidence of breakdown since the same frequencies are observed experimentally at low and high fields and the relative Fourier-transform amplitudes for the frequencies are the same at low and high fields. Thus any breakdown takes place at low fields less than 2 T indicating that the energy gaps are small.

When the $(4\sqrt{3}\times4\sqrt{3})R30°$ superlattice was used there was no possible way to explain all the frequencies observed from dHvA because the size of the intercalant Brillouin zone was much too large with respect to any reasonable fundamental frequencies to provide the overlap of circles from neighboring Brillouin zones. Since x-ray diffraction cannot distinguish between diffraction due to first, second, and third orders from that due to second, fourth, and sixth orders, the intercalant superlattice can also be an $(8\sqrt{3}\times8\sqrt{3})R30°$ superlattice. With the magnitude of the intercalant lattice vectors doubled, the size of the Brillouin zone shrinks in half and provides sufficient overlap to adjust the sizes of the circles to fit the dHvA data.

Previous work on stage-2 $SbCl_5$ intercalated graphite[6] indicated that the two fundamental frequencies were in the ratio of 2.8:1 (1102 T:422 T). This is similar to those of other stage-2 compounds. This ratio between the fundamental frequencies was maintained in this analysis. The lower fundamental frequency was chosen to be 467 T. This value was chosen for three reasons. First, it is close to the low-frequency value for other stage-2 compounds and, second, it is one of the observed frequencies from the de Haas–van Alphen data. The third reason comes from an analysis of the effective masses of the observed dHvA frequencies. The general trend is that the effective mass increases as a function of frequency for one type of carrier. However, the orbit at 467 T does not follow this behavior by having an effective mass larger than the nearest frequencies above and below it. This indicates that this frequency is from a different band than the other frequencies. Therefore, 467 T was chosen as a fundamental frequency. With this choice, the large fundamental frequency was 1320 T in order to maintain the ratio between high and low frequencies. The overlap of these orbits in the first and second Brillouin zones is shown in Figs. 3 and 4. From Fig. 3 we can see that there are two pieces $f_a$ and $f_b$ that result from the overlap of circles for the lower frequency. The areas of these two pieces were determined by
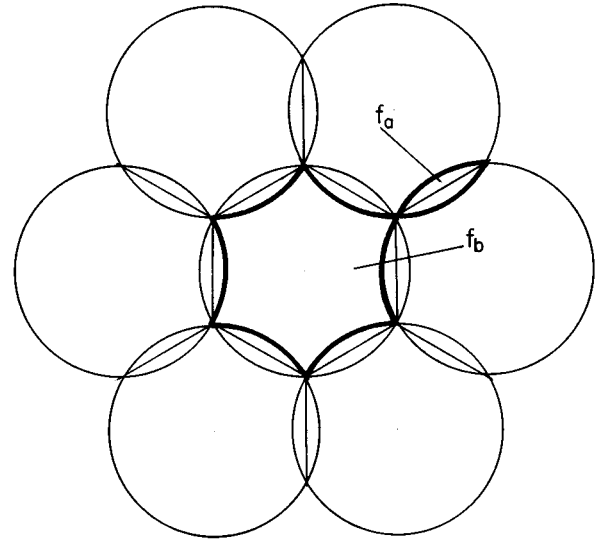


FIG. 3. Circle construction for low-frequency band (467 T).

cutting out and weighing the pieces cut from a paper drawing relative to the area of the fundamental orbit (467 T). The two pieces shown in Fig. 3 each consist of only one type of curvature and so piece $f_a$ can be considered a possible hole orbit and piece $f_b$ can be considered a possible electron orbit.

Figure 4 shows the four pieces created by the overlaps due to the higher-frequency circles. The pieces are labeled $f_1$, $f_2$, $f_3$, and $f_4$. Pieces $f_1$ and $f_3$ each have uniform curvature and so could be electron and hole orbits, respectively, whereas $f_2$ and $f_4$ have mixed curvature and therefore
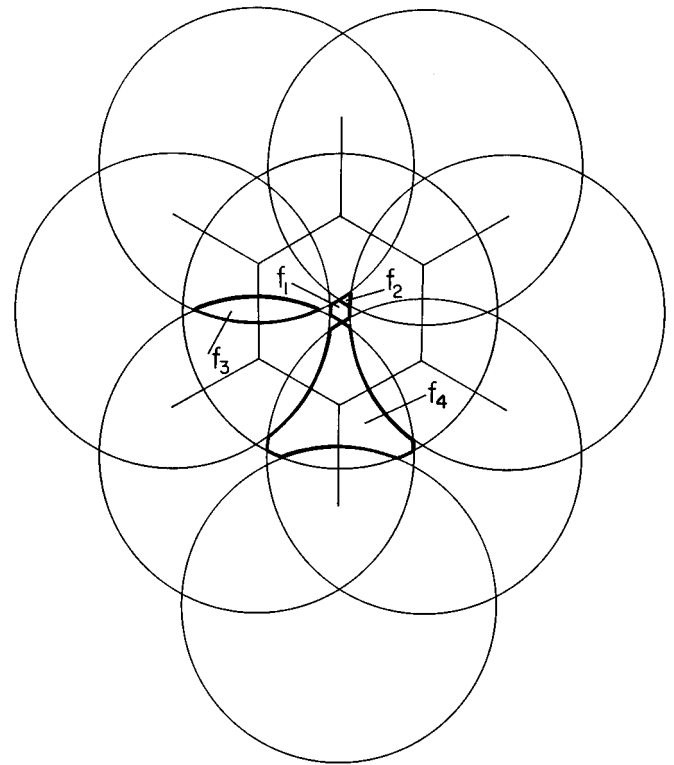


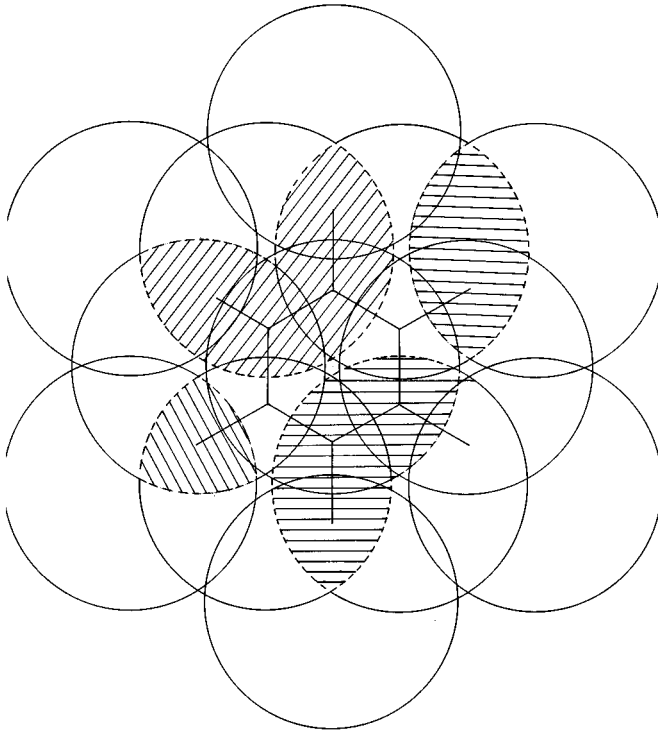FIG. 4. Circle construction for high-frequency band (1320 T).

FIG. 5. Circle construction showing coupled orbits (1320 T).

cannot be considered to be carrier orbits by themselves. However, by combining these pieces in different combinations large carrier orbits can be formed. Figures 5 and 6 show sketches of some of the shapes of the uncoupled orbits from both the high- and low-frequency constructions. In Fig. 5, four possible hole orbits are shown. There are a small three-sided orbit, a lens-shaped orbit, and small and large butterfly-shaped orbits. These orbits correspond to the 256-, 478-, 706-, and 931-T frequencies, respectively. In Fig. 6,
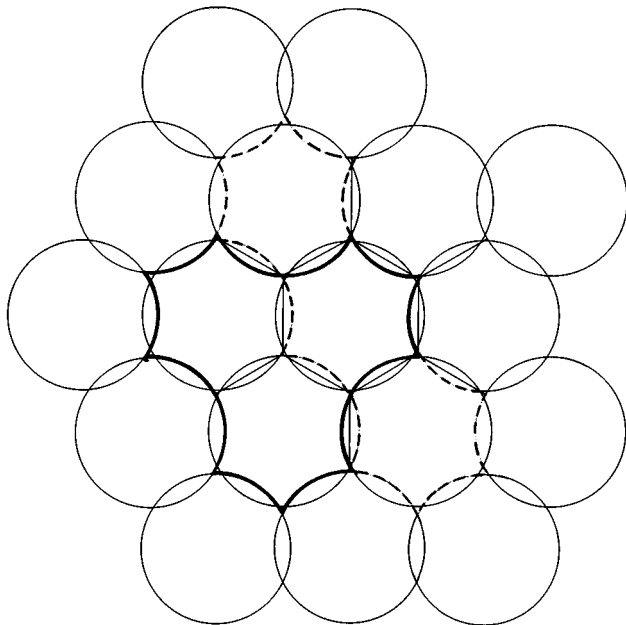


FIG. 6. Circle construction showing coupled orbits (467 T).

TABLE II. dHvA frequencies compared to values calculated by circle construction using the high-frequency (1320-T) band. ($U$) denotes an uncoupled orbit.

| dHvA ($T$) | Calculated frequency | % Difference | Construction |
|---|---|---|---|
| 270 | 256 ($U$) | −4.5 | $f4 + 3f3$ |
| 466 | 478 ($U$) | 2.6 | $2f4 + 5f3 + 2f2$ |
| 515 | 541 | 5.3 | $3f4 + 18f2 + 7f1$ |
| 579 | 564 | −2.6 | $3f4 + f3 + 16f2 + 6f1$ |
| 631 | 588 | −6.8 | $3f4 + 2f3 + 14f2 + 5f1$ |
| 706 | 706 | 0.0 | $3f4 + 7f2 + 4f2$ |
| 891 | 896 | 0.6 | $5f4 + 30f2 + 11f1$ |
| 966 | 931 | −3.6 | $4f4 + 9f3 + 6f2$ |
| 1032 | 1075 | 4.2 | $6f4 + 36f2 + 13f1$ |
| 1089 | 1097 | 0.7 | $6f4 + f3 + 34f2 + 12f1$ |
| 1157 | 1158 | 0.1 | $6f4 + 3f3 + 30f2 + 12f1$ |
| 1217 | 1253 | 3.0 | $7f4 + 36f2 + 15f1$ |
| 1344 | 1336 | −0.6 | $7f4 + 3f3 + 36f2 + 14f1$ |
| 1424 | 1431 | 0.5 | $8f4 + 42f2 + 17f1$ |

two possible electron orbits are shown. The solid line outlines an orbit corresponding to 1073 T and the dashed line corresponds to an orbit with a frequency of 1050 T. Table II shows the frequencies from the dHvA data compared to the frequencies calculated from the circle construction for the high-frequency (1320-T) band and Table III shows the comparison to the frequencies calculated for the low-frequency (467-T) band construction.

Some of these constructions may seem extremely complicated as possible carrier orbits; however, all of the constructions are made up of the pieces seen in Figs. 3 and 4 with some of the larger orbits being a series of these smaller orbits strung together. In all cases, care has been taken to ensure the curvature of the pieces is consistent.

The low-frequency construction is important because it accounts for a good match with the peak at 466 T, which has a large amplitude and an anomalous effective mass. The remainder of the frequencies in the table have a smaller amplitude and are also accounted for from the high-frequency construction except for the peak at 328 T. This peak has a very small amplitude and was only seen as distinguishable from the background in one of the three dHvA spectra.

The zone-folding model provides good identification for nearly all of the frequencies that are observed. However, there are other frequencies provided by the model that are

TABLE III. dHvA frequencies compared to values calculated by circle construction using the low-frequency (467-T) band.

| dHvA ($T$) | Calculated frequency | % Difference | Construction |
|---|---|---|---|
| 328 | 336 ($U$) | 2.4 | $fb$ |
| 466 | 467 | 0.2 | $F$ |
| 706 | 686 | −2.8 | $2fb + fa$ |
| 891 | 911 | 2.2 | $2Fe − fa$ |
| 1032 | 1050 | 1.7 | $3fb + 2fa$ |
| 1157 | 1073 | −7.3 | $3fb + 3fa$ |
| 1344 | 1332 | −0.9 | $3F − 3fa$ |

not observed. There are two very low frequencies predicted at 23 and 34 T that are not observed. These small orbits may not be detected by dHvA or may be shrunk to zero when a potential is included in the model. Also the fundamental frequency of 1320 T is not observed. This is not surprising since in this high-frequency band the orbits created by the zone-folidng effect are dominant. In principle, there are an infinite number of orbits that can result from zone folding. At high frequencies the coupling of many small pieces results in a large number of possible orbits and clearly not all of these can be observed.

It may seem that one could choose any frequency and take complicated combinations in order to satisfy the available orbits but this is not the case. The construction of the orbits is very sensitive to the ratio between the $k_f$, the radius of the free hole Fermi surface in the absence of zone folding, and the length of a side of the Brillouin zone $l_s$. In order to maintain the length $l_s$, determined by the superlattice, and to give reasonable values of the fundamental frequencies, our construction provided the most consistent picture.

The zone folding from the large frequency was tested for values of 1353, 1320, and 1288 T and the values for the four pieces shown in Fig. 5 were compared to the calculated values. The average percent difference for these four pieces is from 10.9% with $F=1288$ T to 3.5% at $F=1353$ T. The average difference for the frequency we have chosen for these peaks is 2.9%, indicating that we have found a value in the minimum of the uncertainty curve. Any more subtle adjustment to further minimize this percent difference was not possible because the uncertainty in the frequencies obtained through the zone-folding calculations is $\pm 1\%$ of each frequency. This value was determined by performing multiple calculations with the same fundamental frequency and comparing the results. In addition, the high-frequency construc-

tion alone can account for all of the observed dHvA peaks to within a maximum difference of 6.8%. The low-frequency construction also provides matches for a number of the peaks with a maximum difference of 7.3% and allows for the explanation of the effective masses of the carriers.

There is only one frequency in the dHvA spectrum that is not explainable by either the low- or high-frequency constructions. This is the frequency at 127 T. It also has an anomalously high effective mass compared with the frequency at 270 T. This is consistent with other stage-2 materials that also have a low-frequency oscillation that is as yet unexplained.

## V. CONCLUSIONS

The de Haas–van Alphen effect of the stage-2 $InCl_3$ graphite intercalation compound was determined with two spectrometers for the magnetic-field ranges of 2–5 and 1–14 T. There was excellent agreement between the data of the two systems. The dHvA frequencies were in the range 126–1424 T and the cyclotron masses were between $0.095m_0$ and $0.27m_0$. There were at least 15 dHvA frequencies observed. All of the frequencies except for 127 T were explained by the zone folding of the Fermi surface for the stage-2 compound by the superlattice of the ordered intercalant. The superlattice periodicity was $8\sqrt{3} \times 8\sqrt{3}R^\circ$ with respect to the graphite lattice.

[1] J. Blinowski, H. H. Nguyen, C. Regaux, J. P. Vieren, R. Letoullec, G. Furdin, A. Herold, and J. J. Melin, J. Phys. (Paris) **41**, 47 (1980).

[2] W. R. Datars, J. Palidwar, and P. K. Ummat, J. Phys. Condens. Matter **7**, 5967 (1995).

[3] E. Stump, Mater. Sci. Eng. **31**, 53 (1977).

[4] W. R. Datars, P. K. Ummat, H. Aoki, and S. Uji, Phys. Rev. B **48**, 18 174 (1993).

[5] L. M. Falikov and P. R. Sievert, Phys. Rev. **138**, A88 (1965).

[6] H. Zaleski, P. K. Ummat, and W. R. Datars, Phys. Rev. B **35**, 2958 (1987).